Dynamic wetting characteristics attributable for pool boiling heat transfer of FeCrAl- and Cr-layered vertical tubes

Hong Hyun Son[1], Yun Sik Cho[1], Sung Joong Kim[1,2*]
[1]*Department of Nuclear Engineering, Hanyang University*
[2]*Institute of Nano Science & Technology, Hanyang University*
222 Wangsimri-ro, Seongdong-gu, Seoul 04763, Republic of Korea
hhson@hanyang.ac.kr, whdbstlr147@hanyang.ac.kr,
[*]*Corresponding author: sungjkim@hanyang.ac.kr*

1. Introduction

Recent studies for a development of accident-tolerant fuel (ATF) cladding have focused on the evaluation of oxidation resistance of candidate coating materials under high temperature steam environments. Most studies [1] have reported that FeCrAl (FCA) and Cr among a series of metals have an outstanding function to resist high temperature steam reaction.

For the further development, however, thermal performance of those candidates needs to be evaluated in terms of boiling heat transfer because well-arranged coating structures in nanoscale possibly leads to the reduction of active nucleation for nucleate boiling and rewetting when approaching the critical heat flux (CHF). In order not to repair the CHF margin, the coated surface needs to bear surface roughness in microscale.

Thus this study focuses on the comparison of nucleate boiling heat transfer coefficient (NBHTC) and CHF between FCA- and Cr-layered tube surfaces having different surface roughness. In order to quantify NBHTC and CHF, pool boiling experiment was conducted with vertically heated tubes. In essence, the CHF enhancement was analyzed through dynamic wetting behavior and morphological change.

2. Fabrication of FCA- and Cr-layered tube surfaces

Tube surfaces were polished with 800 and 60 grits of sandpaper before sputtering. Generally, lower grit number generates higher surface roughness. Then contaminants on the polished surfaces were carefully removed using an ethanol solution.

FCA and Cr deposition was conducted using a DC magnetron sputtering. The sputtering conditions are summarized in Table I. The sputtering process was carried out at an 150 ^{o}C substrate temperature for 1 hr.

Table I: DC sputtering conditions

Sputtering parameter	Target condition
Target material	FeCrAl (75:20:5 wt%) Cr (99.95 % purity)
Substrate material	Stainless steel grade 316L tube
Substrate temperature (^{o}C)	150
Exposure time (hour)	1
Working pressure (Torr)	1×10^{-2}
DC power (W)	150 – 160

Figure 1 shows (a) the thin film and (b) the change of surface morphology before and after DC sputtering. During an hour of sputtering, an approximately 1 μm thin film was formed with columnar grains. The morphology of nanostructure was formed differently for FCA- and Cr-layered surfaces. FCA-layered surface consists of grain-based nanostructures while nanostructure of Cr-layered surface shows particulate shape with ~200 nm in size.

Interestingly, those nanostructures make FCA-layered surfaces hydrophilic (29^{o}~35^{o}) and Cr-layered surfaces superhydrophilic (~0^{o}). It implies that particulate nanostructures contribute to further enhancement of hydrophilicity. However, the difference of surface morphology by the change of roughness was not observed.

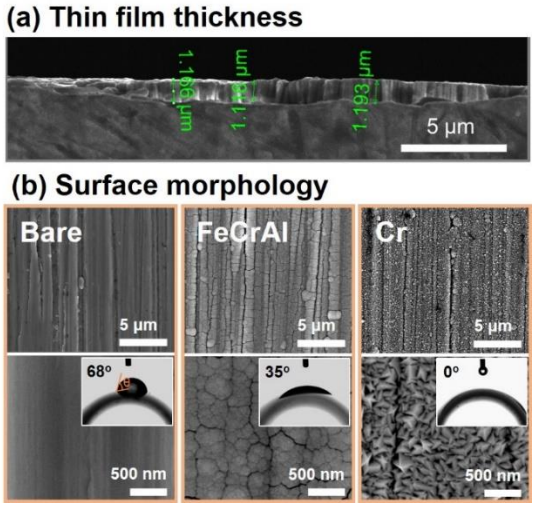

Fig. 1. SEM images: (a) thin film thickness; (b) surface morphology.

3. Experimental description

Figure 2 shows pool boiling apparatus and detailed design of the test section. In order to apply heat into tube, Joule heating method was adopted. Two K-type thermocouples were inserted into a TC guide tube and held at 10 mm distance from the top and the bottom. For quantification of NBHTC and detection of CHF, the top-

located TC was used because CHF repetitively occurred at the top position. Void between a tube heater and a TC guide tube was filled with an epoxy for thermal and electrical insulation.

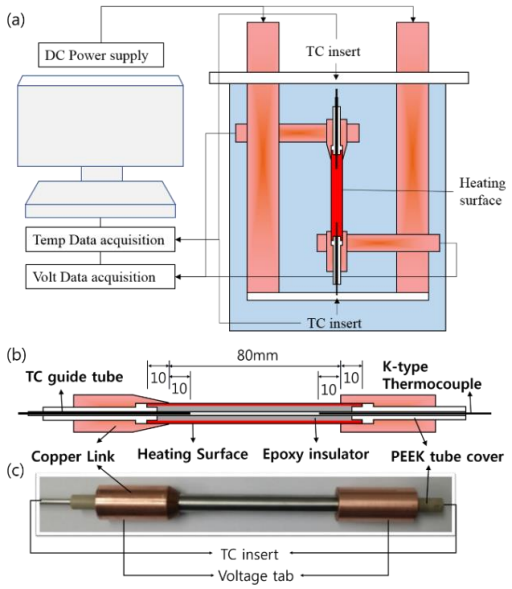

Fig. 2. (a) Pool boiling apparatus; (b) cross-sectional schematic of test section; (c) photo of test section.

The tube length, outer diameter, and tube thickness are 100 mm, 9.52 mm, and 0.88 mm, respectively. Here, active heated length is 80 mm because the both end length of 10 mm is used to electrically contact with copper electrodes.

Applied heat flux was calculated using a simple heat flux equation as shown in Eq. (1).

$$q'' = \frac{Power}{A_{heated}} = \frac{VI}{\pi D_o L_{heated}} \quad (1)$$

V is the voltage drop across the length of the heater, I is the current, D_o is the outer diameter of tube, and L_{heated} is the heated length. Using a propagation of error method, measurement uncertainty was estimated as 5.5%.

4. Result and discussion

4.1 NBHTC and CHF

As shown in Fig. 3(a), NBHTC of FCA-SP800 increased by 24% at high heat flux (~ 636 kW/m^2) while NBHTC of Cr-SP800 decreased by 10%. In case of SP60, the effect of FeCrAl layer on NBHTC was almost vanished showing similar trends with B-SP60. Contrary to FCA-SP60, NBHTC of Cr-SP60 was approximately 15% lower than B-SP60.

It is well known that superhydrophilic nature reduces active nucleation for nucleate boiling because superhydrophilic cavities require higher nucleation pressure than hydrophilic surfaces. This relation can be confirmed by Young-Laplace equation (Eq. (2)) as follows.

$$\Delta P = \frac{2\sigma \cos\theta_e}{r} \quad (2)$$

Here, σ is the surface tension of liquid, θ_e is the equilibrium contact angle, and r is the radius of cavity mouth. In this equation, a decrease of equilibrium contact angle is directly related to an increase of nucleation pressure. Thus, more heat flux should be applied to activate micro-cavities for bubble nucleation. On the contrary, nucleation pressure of hydrophilic surfaces is lower than superhydrophilic surfaces.

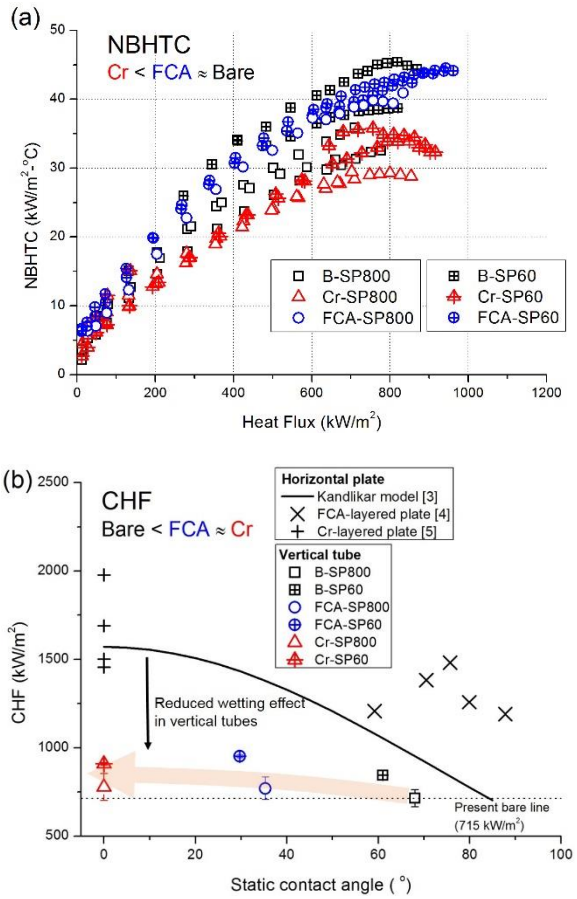

Fig. 3. (a) NBHTC trend and (b) CHF comparison with Kandlikar model [3] and open data [4, 5]. Note that sputtering conditions of open data (plate sputtering) are different with present conditions (tube sputtering), although DC magnetron sputtering technique was applied evenly.

However, Young-Laplace equation is applicable for certain limit of nucleation at given cavity sizes. Accordingly, the equation does not include the physical relation of contact angle with bubble dynamics such as bubble growth and departure. Thus, more information is needed to define exact relation between NBHTC and contact angle.

Phan et al. [2] showed that for an increase of contact angle bubble departure diameter decreases whereas bubble emission frequency increases. In their experiments, nucleate site density hardly changed with contact angle but unlike current experiment

superhydrophilic surface was not considered. By combining those relations, they further predicted that NBHTC of superhydrophilic surface becomes higher than hydrophilic surface. However this prediction is opposite to current result. Although not included in this paper, we have observed highly reduced active nucleation using high-speed visualization in case of Cr-layered superhydrophilic surfaces. Thus, we believe that the reduced active nucleation of superhydrophilic surfaces plays an important role in decreasing NBHTC. This will be evaluated in the future.

Regardless of the deteriorated NBHTC, compared to the CHF of bare specimen (B-SP800), CHF of FCA- and Cr-layered surfaces was enhanced by 34% and 27%, respectively. Moreover, an increase of surface roughness caused more CHF enhancement. In Fig. 3(b), present data were compared with Kandlikar model [3] and open source [4, 5]. Kandlikar model mainly considers force balance of a growing bubble between vapor recoiling and surface tension at the bubble base. In Eq. (3), arranged form indicates that CHF increases with a decrease of contact angle.

$$q''_{Kandlikar} = K \times h_{fg} \rho_g^{1/2} \left[\sigma_{lv} g \left(\rho_l - \rho_g \right) \right]^{1/4}$$
$$K = \left(\frac{1+\cos\theta_r}{16} \right) \left[\frac{2}{\pi} + \frac{\pi}{4} \left(1+\cos\theta_r \right) \cos\psi \right]^{1/2} \quad (3)$$

Our result also shows an increasing CHF trend with a decrease of contact angle, although the enhancement ratio was lower than Kandlikar's prediction. It is possibly due to the reduced wetting effect, which comes from the difference of heater geometry. Unlike horizontal plate, for vertical tube buoyancy-driven flow along axial direction causes premature bubble departure, formation of a lump of vapor, and consequently, an increase of void fraction downstream, in which CHF occurs. Likewise, open data obtained from horizontal plate showed higher enhancement than present data.

Above hydrodynamic factors are not of interest in this study. Moreover, a static contact angle alone hardly clarifies the cause of CHF enhancement in the explored surfaces. Thus, in the next section, we will mainly discuss the cause of CHF enhancement in terms of dynamic wetting behavior and morphological changes.

4.2 Dynamic wetting

Recently, observations of boiling structures using infrared cameras have improved understanding of pool boiling CHF mechanism. According to the experimental observations, the CHF occurs when liquid inflow sucked into microlayer around dry spots is completely evaporated, forming irreversible dry patches. Figure 4 simply shows a physical concept of microlayer evaporation model in which the growth of dry spot mainly competes with liquid inflow. Thus, more liquid inflow is given, reversible dry spots are vanished, which contributes to CHF enhancement.

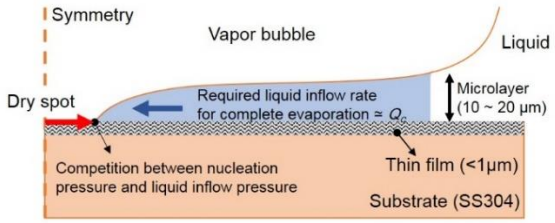

Fig. 4. Schematic of microlayer evaporation model.

As an analytical approach to resolve a hydrodynamic analogy between liquid suction in microlayer and CHF triggering, Rahman et al. [6] introduced a physical concept, which describes that the maximum wicked volume flux ($\dot{V}''_0$) of textured surfaces is proportional to CHF enhancement ratio. In Eq. (4), this parameter is expressed as the combination of maximum volume flow rate, $(dV/dt)_{t=0}$, and apparent wetted area A_w.

$$\dot{V}''_0 = \frac{1}{A_w} \left(\frac{dV}{dt} \right)_{t=0} \quad (4)$$

Evidently, wicked volume flux is the one of dynamic wetting phenomena. However, it is difficult to measure readily because additional capillary tubes are needed to quantify wicked volume rate. Moreover, this method seems applicable for capillarity-dominant surfaces, whose property is not considered as major wetting factor in explored surfaces.

In this regards, we similarly focused on spreading behavior, a kind of dynamic wetting, of a water droplet on tube surfaces. In this approach, volumetric liquid inflow rate Q_c can be expressed as follows.

$$Q_c \cong u_a A_c N_c \quad (5)$$

where u_a is the advancing rate of a water droplet, A_c is the cross-sectional area of microflow channel, and N_c is the number of microflow channels. Here, the microflow channel means the micro-scratched lines on differently-polished tube surfaces, which is depicted in Fig. 5(b).

The advancing rate of a water droplet, u_a, was quantified by calculating the slope of increasing liquid contact diameter when a water droplet spreads over tube surfaces. Figure 5(a) shows the increasing trend of the contact diameter for each surface. The repetitive measurement of the advancing rate results in 0.20 m/s, 0.39 m/s, and 0.48 m/s on bare, FCA-, and Cr-layered surfaces, respectively. The enhanced advancing rate on FCA- and Cr-layered surfaces comes from the existence of nanostructures because the intrinsic contact angle of SS316L, FCA, and Cr is almost the same. In addition, the more particulate nanostructures of Cr layer than FCA layer (Fig. 1(b)) contributes to the more enhanced liquid spreading.

Interestingly, for all surfaces, roughness effect on the advancing rate was not observed. It implies that for the explored surfaces liquid spreading momentum is strongly governed by nanostructures rather than micro-

scratches. In other words, the effect of capillary pumping by the change of surface roughness seems negligible.

The cross-sectional area of microflow channel $A_c=2R_aR_{sm}$ was calculated by a product of R_a and R_{sm}. Here, $4R_a$ and R_{sm} represent the height and the width of the unit channel, respectively. Morphologically, the number of microflow channel N_c corresponds to the number of peaks along roughness profile. Thus, it is assumed that the number of microflow channel N_c is proportional to $1/R_{sm}$. Final expression of volumetric liquid inflow rate is as follows.

$$Q_c \cong 2u_a R_a \quad (6)$$

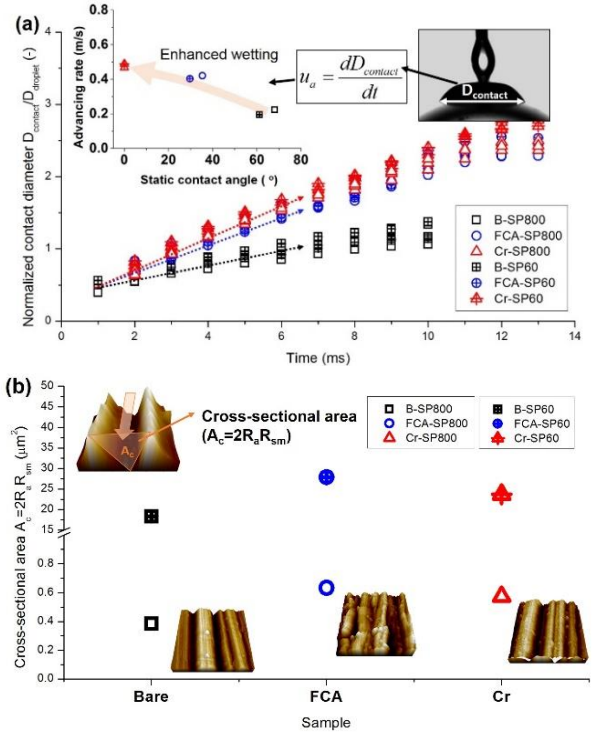

Fig. 5. Quantification of volumetric liquid inflow rate: (a) dynamic wetting behavior measured using high-speed imaging; (b) morphological changes of cross-sectional area A_c measured by AFM.

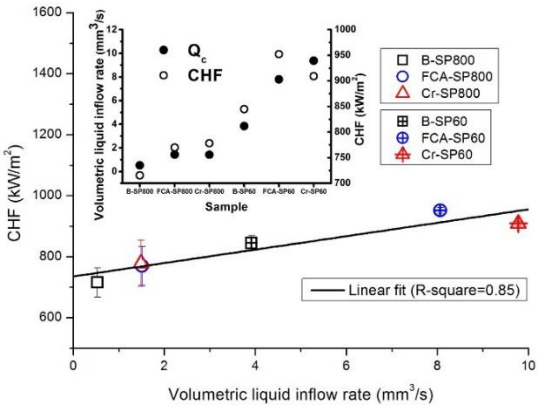

Fig. 6. CHF enhancement as a function of volumetric liquid inflow rate, Q_c.

Figure 6 shows that the CHF values linearly follows Eq. (6). It means that dynamic wetting analysis based on liquid spreading substantially agrees with the microlayer evaporation model although the linearity of the trend seems not completely satisfied due to insufficient R-square value of 0.85.

5. Conclusions

Hydrophilicity of FCA layer resulted in enhancement of NBHTC and CHF. In contrast, superhydrophilicity of Cr layer reduced NBHTC while enhancing CHF. The reduction of NBHTC on Cr-layered surfaces could be attributed to the reduced active nucleation due to highly-wetting surface morphology in nanoscale.

The CHF trend was analyzed on the basis of the microlayer evaporation model. By quantifying dynamic wetting behavior and morphological change, it was observed that the increasing volumetric liquid inflow rate shows a good agreement with the CHF values. However, its linearity was not completely clear in current stage.

As a future work, more analytical investigation is needed to elucidate a hydrodynamic analogy between dynamic wetting and CHF triggering in terms of morphological change.

ACKNOWLEDGEMENT

This research was supported by the Basic Science Research Program through the National Research Foundation of Korea (NRF) funded by the Ministry of Science, ICT & Future Planning (No. 2015R1C1A1A01054861), and by the National Research Foundation of Korea (NRF) grant funded by the Korean government (MSIP) (No. 2016R1A5A1013919).

REFERENCES

[1] S. Bragg-Sitton, Development of advanced accident-tolerant fuels for commercial LWRs, Nuclear News, Vol. 57, p. 83, 2014.

[2] H. T. Phan, N. Caney, P. Marty, S. Colasson, and J. Gavillet, How does surface wettability influence nucleate boiling?, C. R. Mecanique, Vol. 337, pp. 251-259, 2009.

[3] S.G. Kandlikar, A theoretical model to predict pool boiling CHF incorporating effects of contact angle and orientation, Journal of Heat Transfer, Vol. 123, pp. 1071-1079, 2001.

[4] G. W. Seo, G. Jeun, and S. J. Kim, Enhanced pool boiling critical heat flux with a FeCrAl layer fabrication by DC sputtering, International Journal of Heat and Mass Transfer, Vol. 102, pp. 1293-1307, 2017.

[5] H. H. Son, G. H. Seo, and S. J. Kim, Enhanced pool boiling critical heat flux induced by capillary wicking effect of a Cr-sputtered superhydrophilic surfaces, Transactions of the Korean Society Autumn Meeting, Oct. 27-28, 2016, Gyeongju, Korea.

[6] M.M. Rahman, E. Ölçeroğlu and M. McCarthy, Role of Wickability on the Critical Heat Flux of Structured Superhydrophilic Surfaces, Langmuir, Vol. 30, pp. 11225-11234, 2014.